Ultrafast Dynamic Compression Technique to Study the Kinetics of Phase Transformations in Bismuth

R. F. Smith, J. H. Eggert, M. D. Saculla, A. F. Jankowski, M. Bastea, D. G. Hicks, and G. W. Collins

Lawrence Livermore National Laboratory, P.O. Box 808, Livermore, California 94550, USA

Preheated Bi (296–532 K) was ramp compressed with 15–35 ns rise times to a peak stress of ~11 GPa to explore structural phase-transformation kinetics under dynamic loading conditions. At high strain rates, $\dot{\varepsilon} > 5 \times 10^6$ s^{-1}, deviation from equilibrium phase boundaries suggests that compression time scales are comparable to the new phase incubation period. The dependence of $\Delta P/kT$ on $\dot{\varepsilon}$ is consistent with a thermally activated transformation.

Pursuit of a detailed understanding of pressure-induced structural phase-transformation kinetics has been an active area of theoretical and experimental research in condensed-matter physics for several decades [1–9]. Despite this, there remains a lack of quantitative data primarily due to the limitations in experimental techniques to measure these extremely rapid phenomena. Studies of time-dependent transformations have typically used shock-compression, in which a single point in stress-temperature (P_x-T) space is reached over the shock-wave rise time. If P_x lies beyond a phase boundary a two-wave profile propagating in the sample can develop due to wave speed differences between the two phases. Measurement of the intermediate temporal slope connecting this two-wave structure has been used to infer phase-transformation time scales [5].

Recently developed ramp-wave-loading (RWL) techniques offer greater sensitivity over shock experiments in detecting phase transformations [6,7]. Here, we use laser-driven RWL of 20–50 μm thick preheated Bi foils to sample continuous paths in P_x-T space. These experiments represent, to our knowledge, the first time multiple-wave features associated with phase transformations have been observed under laser-driven compression. The time scale for laser-driven RWL [10] is several to tens of nanoseconds, substantially shorter than previously reported phase transition times for Bi I-II [7–9]. By preheating the Bi (296–532 K) different paths through P_x-T space are explored to provide insight into the phase-transformation mechanisms. Under these rapid compression time scales, the equilibrium Bi I-II phase boundary is determined to be overpressurized by $\Delta P \sim 0.3$–1 GPa. The onset of significant growth of $\Delta P/kT$ occurs at a threshold strain rate, $\dot{\varepsilon}_0 = \frac{d\ln V}{dt}$, of 5×10^6 s^{-1}. For higher $\dot{\varepsilon}$, $\Delta P/kT$ increases logarithmically. The growth of $\Delta P/kT$ for $\dot{\varepsilon} > \dot{\varepsilon}_0$ suggests compressing on time scales comparable to the new phase incubation period [2].

The laser-driven RWL target design consists of a 125 μm polyimide [C$_{22}$H$_{10}$N$_2$O$_5$] foil, a 325–400 μm vacuum gap, and the Bi/window target (Fig. 1). One beam of the Janus laser at 527 nm delivered 150–200 J in a 4 ns square pulse onto the polyimide which generated an ablatively driven shock. A kinoform phase plate inserted into the beam line produced a ~1 mm square, planar ($\Delta I/I \sim 5\%$) region at the focal plane. After shock break-out from the rear surface, the polyimide rarefies across the vacuum gap, loads up against the Bi sample, and launches a ramp-compression wave. The Bi was coated onto either a LiF [100] or sapphire [001] window under conditions which yielded a grain size of ~5 μm in the stress loading direction and ~1 μm in plane [11]. The Bi rhombohedral crystal structure was orientated along the c axis [001] in the growth direction with random orientation in plane and was measured to be fully dense (9.78 g/cc) to within an accuracy of 0.6%. The time history of the transmitted compression wave was recorded by measuring the Bi/window interface velocity $u(t)$ with a line-imaging velocity interferometer system for any reflector (VISAR) with a velocity accuracy of ~10 m/s and a streak camera temporal resolution of ~0.1 ns [12]. The interface velocities were corrected for the stress dependence of the windows' refractive indices [13].
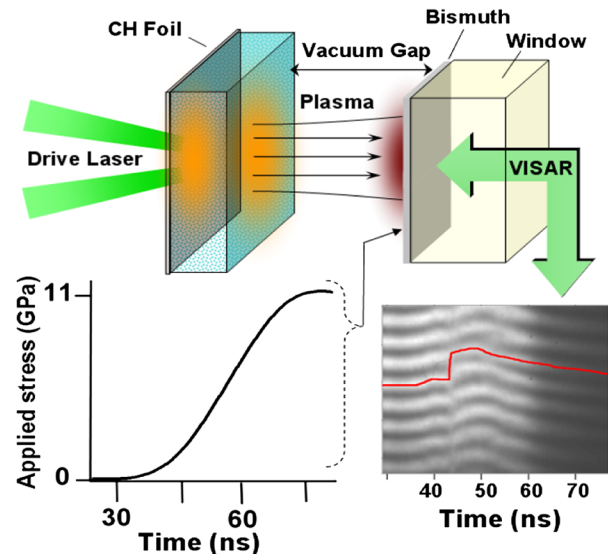

FIG. 1 (color online). Target design for laser-driven ramp compression of a Bi foil.

The loading history $P_x(t)$ was estimated by replacing the Bi/window target with an Al/LiF target. By measuring $u(t)$ at the impedance-matched Al/LiF interface and integrating the equations of motion backwards in space, using the equation-of-state of aluminum, $P_x(t)$ can be estimated for any laser irradiation-target configuration [14]. The ramp rise times (15–35 ns) and peak P_x (8–11 GPa) used here, are a function of vacuum gap size and laser energy.

The initial Bi temperature, T_i, was controlled by resistive heating, to an accuracy of ± 5 K to explore different regions of P_x-T space. The output from the line-imaging VISAR, $u(x,t)$, is shown in Fig. 1 for a Bi/sapphire sample, with $T_i = 463$ K. Shown in Fig. 2 are recorded Bi/LiF and Bi/sapphire interface velocity histories for T_i spanning 296–495 K. All velocity profiles are characterized by a smooth ramp with a shoulder followed by a plateau and a fast rise. The shoulder-point velocity u_{sp} decreases with increasing T_i.

The transformation from the smoothly rising load profile in Fig. 1 to the structured transmitted wave profiles in

Fig. 2 is understood by considering the target dynamics in Lagrangian coordinates (Fig. 3). $P_x(t)$ may be represented by a characteristic (x-t trajectory) propagating through the Bi sample with a slope inversely proportional to the Lagrangian sound speed, $C_L = \frac{\rho}{\rho_0}(\frac{\partial P_x}{\partial \rho})^{1/2}$. When $P_x(t)$ coincides with the equivalent hydrostatic pressure, P, associated with the Bi I-II phase boundary the material enters a mixed phase region. The resultant drop in C_L causes a separation of characteristics and a shoulder point followed by the plateau on the recorded Bi/LiF interface velocity, $u(t)$. In our analysis we use u_{sp} as a signature of the onset of higher phases ($>$Bi I). The observed drop in u_{sp} with T_i is related to the negative P-T slope of the Bi I-II phase boundary. When the rate of compression is comparable to the incubation period for the phase transformation, an evolving mixed phase region exists over a range of P_x resulting in a "ramped" plateau for LiF windows. Once fully transformed from Bi I into a higher phase, C_L increases generating a shock and a fast $u(t)$ rise. For the sapphire window targets, impedance matching at the Bi/sapphire interface increases the interface stress. Thus, the phase transition in Bi will originate both at the drive surface and at the Bi/sapphire interface. It is the transition at the Bi/sapphire interface that we observe, leading to the flat plateau for sapphire windows. The values of u_{sp} are markedly different for the LiF and sapphire windows ($\sim 2x$; see Fig. 2). Only by extracting the stress at the phase transition in the Bi by impedance matching do we obtain consistency between the data for the two window materials, as discussed below.

u_{sp} is related to an equivalent particle velocity, hydrostatic pressure, density, and strain rate $\dot{\varepsilon}$ [15] within the bulk Bi sample by using an analytic Bi I equation of state
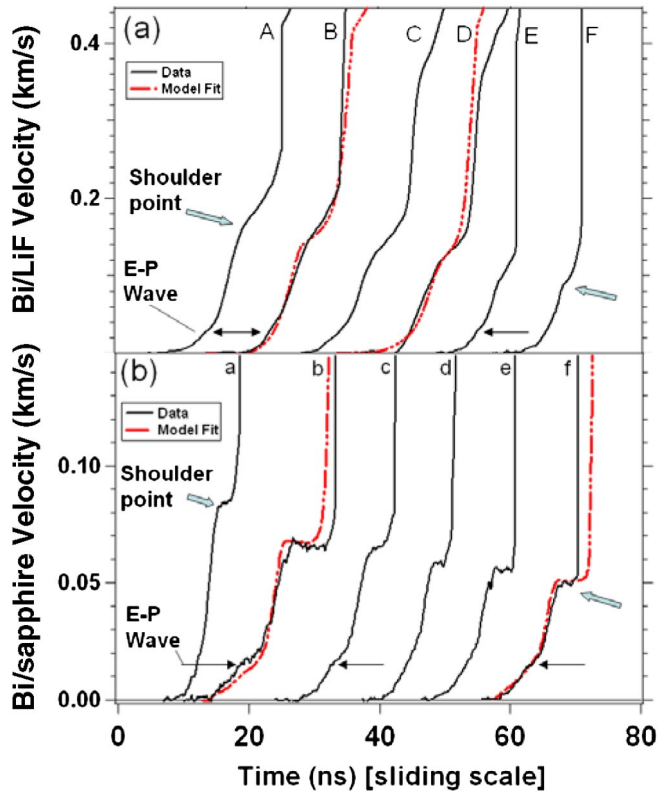

FIG. 2 (color online). The time histories for the (a) Bi/LiF interface velocity with T_i (A–F) of 296, 349, 443, 467, 493, and 495 K, respectively, and (b) the Bi/sapphire interface velocity with initial T_i (a–f) of 296, 343, 393, 443, 463, and 476 K, respectively. The 463 K (e) profile was extracted from the VISAR data shown in Fig. 1. Trace b was a 50 μm thick sample as opposed to the standard 20 μm thick samples. Also shown are velocity profiles calculated from the nonequilibrium model described by Kane *et al.* [22] using the input pressure profile from Fig. 1.
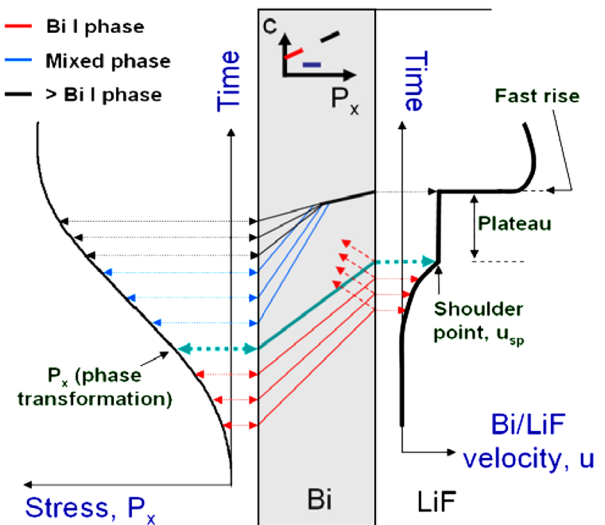

FIG. 3 (color online). A characteristics view of wave propagation through a Bi/LiF sample. Upon entering the mixed phase region there is a drop in the material sound speed, which causes a separation of the characteristics, and produces a shoulder point followed by a plateau on the measured Bi/LiF interface velocity.

(EOS) [16] with a perfectly elastic to perfectly plastic transition determined by our data, and assuming an elastic EOS for both sapphire ($P_x = 44.2u_p + 4.7u_p^2$ [17]) and LiF ($P_x = 17.35 \, u_p + 6.23u_p^2$ [18]) with P_x and u_p in GPa and km/s, respectively. Because of impedance matching between Bi and the LiF window, incoming stress waves are released upon reflection at the window. Thus, the observed plateau for LiF windows corresponds to the phase transition originating at the drive surface. The impedance matching is performed by solving for the P_x-u_p corresponding to a forward-going ramp in the window and a forward- and backward-going ramp in the bismuth. The intersection of backward- and forward-going ramps in the Bi gives the bulk-Bi u_p. The samples are sufficiently thick that the reflected waves from the Bi/LiF interface do not reach the initial loading surface until late times. For the Bi/sapphire samples, the plateau we observe is associated with the transition originating at the Bi/sapphire interface, so no impedance matching is required and the stress is given directly by the sapphire $P_x(u_{sp})$ relation.

Since these experiments are uniaxially loaded, $P_x(u_{sp})$ needs to be related to hydrostatic pressure, P_{sp}, in order to draw comparison against equilibrium phase boundaries. In the analysis of Fowles [19] the stress deviation between P_x and P above yielding corresponds to two-thirds the yield strength Y. For an elastic-plastic material, $Y = (1 - 2\nu)/(1 - \nu)*P_{x(E-P)}$ [19]. Here, $P_{x(E-P)}$ is the elastic-plastic (E-P) transition stress and Poisson's ratio ν is assumed constant at 0.34 over the temperature range studied [20]. The average u_{E-P} measured for the Bi/LiF and Bi/sapphire targets (see Fig. 2) are 0.031 ± 0.006 km/s and 0.015 ± 0.003 km/s, respectively, and are observed to be approximately constant across the T_i range sampled (Fig. 2). Impedance matching yields $P_{x(E-P)}$ of 0.61 ± 0.12 GPa (LiF) and 0.50 ± 0.10 GPa (sapphire) and Y of 0.31 ± 0.06 GPa (LiF) and 0.25 ± 0.05 GPa (sapphire). To correct the data to a hydrostatic pressure we use an average Y value of 0.27 ± 0.04 GPa. This is ∼5 times higher than has been previously reported on shock experiments [8]; similarly high E-P transitions were observed in aluminum [10]. The insensitivity of Y to temperature suggests no thermal softening of the preheated Bi sample. This is in contrast to the reported eightfold decrease in the yield strength of Bi when heated close to melt and stressed over 9 orders of magnitude more slowly [21]. The error bars for P_{sp} shown in Fig. 4 reflect the uncertainty in measuring u_{sp} and determining Y.

The inferred P_{sp}-T points are shown in Fig. 4 alongside the Bi I, II, and liquid equilibrium phase boundaries [22]. To estimate the temperatures plotted in Fig. 4 an isentrope $T(P)$ is constructed through T_i using the Bi I EOS [16]. This technique of converting the u_{sp} to a point in P_{sp}-T space does not require *a priori* knowledge of $P_x(t)$ at the loading surface or an exact knowledge of the target thickness. No estimates were made of plastic work heating. Under the ultrafast time scales reported here, the inferred
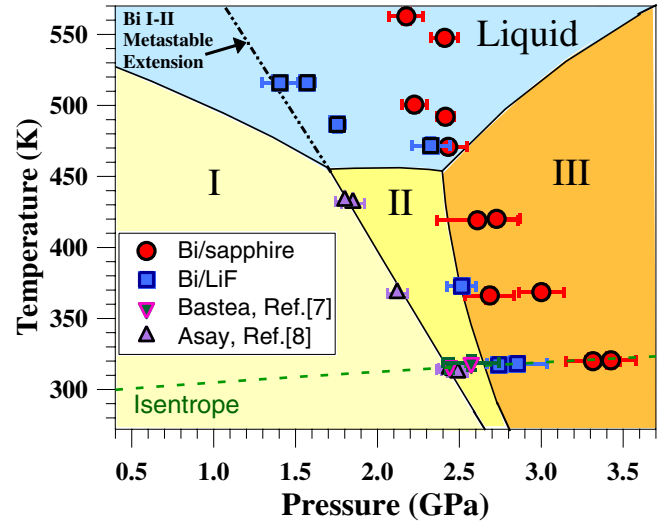

FIG. 4 (color online). P-T plot of Bi shown with I, II, and liquid equilibrium phase boundaries. Points from a series of preheated Bi samples are shown for the two different window materials used (LiF, sapphire) along with the points taken by Bastea [7] and Asay [8].

P_{sp}-T points lie at higher pressures than the Bi I-II equilibrium phase boundary by ∼0.3–1 GPa.

The ability to control T_i enables different regions of the Bi I-II phase boundary to be explored and gives insights into the temperature dependence of the transformation. Figure 5 shows the overpressurization, ΔP, divided by kT versus the strain rate at the Bi I-II equilibrium phase boundary [15]. $\Delta P = P_{sp} - P_{\text{I-II equil}}$ along the isentrope and the errors in ΔP come directly from the determination of P_{sp} since the uncertainties in the Bi I-II equilibrium boundary are small and are not considered here [16]. For trajectories above the Bi I-II-liquid triple point, the compression traverses the Bi I-liquid equilibrium phase boundary. No multiwave features at pressures associated with the melt line are observed in our data which suggests that for the $\dot{\varepsilon}$ reported here no significant melting occurs. In the case of slow melt we follow the analysis of Johnson [16] and calculate ΔP for these high-temperature points from the difference between the estimated value of P_{sp} and the metastable extension of the Bi I-II equilibrium boundary (Fig. 4).

We identify a threshold strain rate $\dot{\varepsilon}$ of 5×10^6 s^{-1} above which $\Delta P/kT$ scales logarithmically with $\dot{\varepsilon}$. For strain rates below ∼5×10^6 s^{-1} there is no significant overpressurization of the Bi I-II equilibrium phase boundary. The correlation of $\Delta P/kT(\dot{\varepsilon})$ over the range of T and $\dot{\varepsilon}$ measured here suggests a thermally activated transformation. The data in Fig. 5 are fit to an Arrhenius equation: ($\ln\dot{\varepsilon} = \ln\dot{\varepsilon}_0 + A(\Delta P/kT)$), where the constants $\ln\dot{\varepsilon}_0$ and A are 15.6 ± 0.1 and 0.04 ± 0.006 eV/GPa, respectively [12]. This logarithmic dependence of $\Delta P/kT$ with $\dot{\varepsilon}$ for the Bi I-II transformation is similar to that seen in Ti and Yb for strain rates that were 9 orders of magnitude slower [2].
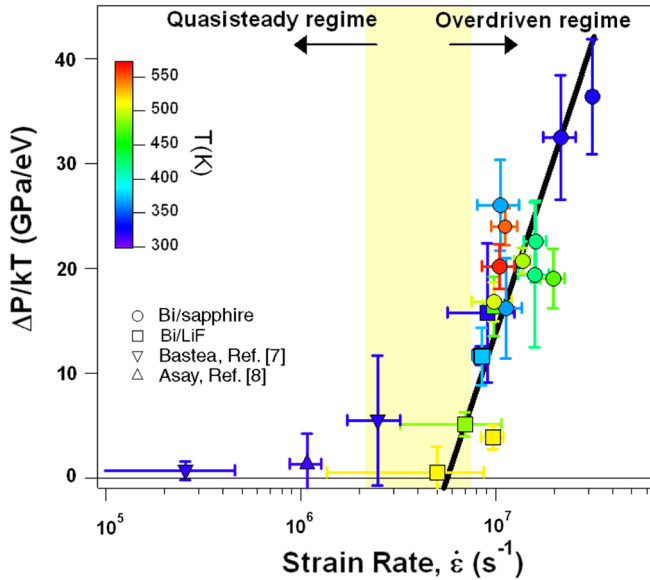
FIG. 5 (color online). $\Delta P/kT$ as a function of strain rate across equilibrium Bi I-II equilibrium phase boundary.

The Bi/window $u(t)$ profiles were modeled, following Kane *et al.* [22], using a 1D hydrocode coupled to a multiphase Bi EOS and a kinetics model to advance the material elements in (P, T, z) space, where the components of the vector z are the mass fractions of the individual phases. This dynamic model qualitatively reproduces the observed VISAR records including the sloped and flat plateaus followed by the fast rise for both the LiF and the sapphire windows, respectively, as shown in Fig. 2. The calculated full transformation time from the Bi I phase τ, when compressed initially along the room temperature isentrope for $\dot{\varepsilon} \sim 10^7$ s^{-1}, is $\sim$3 ns. Applying the same kinetics model to the substantially slower ramps employed by Bastea *et al.* [7] suggests a completion time $\tau \sim 60$ ns, consistent with [7]. Including the quasihydrostatic experiments of Getting [9] and Singh [23], we find that τ is strongly correlated with $\dot{\varepsilon}$ over 16 orders of magnitude in strain rate, and a fit to all the reported $\tau(\dot{\varepsilon})$ data for Bi I-II reveals a $\tau = 0.007\dot{\varepsilon}^{-0.379}$ dependence. Interestingly, only at $\dot{\varepsilon}_0 \sim 5 \times 10^6$ s^{-1} does ΔP become significantly >0. For $\dot{\varepsilon} > \dot{\varepsilon}_0$ the transformation is overdriven which suggests that compression rise times are comparable to the new phase incubation period. Within this regime the transformation follows an Arrhenius behavior suggestive of a thermally activated energy barrier. The incubation period is thought to be related to the formation of new phase nuclei, and has been observed by Singh [2] to decrease logarithmically with ΔP for Ti and Yb.

We have employed a laser-driven RWL technique at high strain rates to study time-dependent effects on phase transformations in Bi. Preheating enables access to different regions of P-T space and provides insights into the phase-transformation mechanisms. $\Delta P/kT$ is shown to have a logarithmic dependence on the strain rate $\dot{\varepsilon}$ above

a threshold value of about 5×10^6 s^{-1} which is consistent with compression time scales becoming comparable to the new phase incubation period. The ramp rise times reported here are $\sim$10 times faster than previously reported in RWL experiments providing a new experimental technique for studying phase-transformation kinetics.

[1] M. Avrami, J. Chem. Phys. **7**, 1103 (1939).
[2] A. K. Singh, Mater. Sci. Forum **3**, 291 (1985).
[3] N. V. Chandra Shekar and K. Govinda Rajan, Bull. Mater. Sci. **24**, 1 (2001).
[4] M. D. Knudson and Y. M. Gupta, J. Appl. Phys. **91**, 9561 (2002).
[5] J. C. Boettger and D. C. Wallace, Phys. Rev. B **55**, 2840 (1997).
[6] D. H. Dolan *et al.*, Nature Phys. **3**, 339 (2007); M. Bastea *et al.*, Phys. Rev. B **75**, 172104 (2007).
[7] M. Bastea *et al.*, Phys. Rev. B **71**, 180101(R) (2005).
[8] J. R. Asay, J. Appl. Phys. **45**, 4441 (1974); J. R. Asay, J. Appl. Phys. **48**, 2832 (1977).
[9] I. C. Getting, Metrologia **35**, 119 (1998).
[10] R. F. Smith *et al.*, Phys. Rev. Lett. **98**, 065701 (2007).
[11] A. F. Jankowski *et al.*, Mater. Sci. Eng. A **431**, 106 (2006).
[12] P. M. Celliers *et al.*, Rev. Sci. Instrum. **75**, 4916 (2004).
[13] D. B. Hayes, J. Appl. Phys. **89**, 6484 (2001); D. B. Hayes *et al.*, J. Appl. Phys. **94**, 2331 (2003).
[14] See R. F. Smith *et al.*, Phys. Plasmas **14**, 057105 (2007), and references within.
[15] The strain rate, $\dot{\varepsilon} \equiv \frac{d \ln V}{dt}$, was calculated directly from the density obtained by backward propagation of the wave profile to the relevant region of the sample where the phase transition occurred for each window. For Bi/LiF, $\dot{\varepsilon}$ is averaged from the loading surface to a point in Lagrangian space where window reflections do not perturb the incoming ramp. For Bi/sapphire, $\dot{\varepsilon}$ is averaged over 5% of the total target thickness at the Bi/sapphire interface. For both LiF and sapphire windows the averaged $\dot{\varepsilon}$ takes into account the uncertainties in the measurement of P_{sp}, as shown in Fig. 4. The same analysis approach was applied to the data of Bastea *et al.* [7] and Asay [8].
[16] J. N. Johnson *et al.*, J. Phys. Chem. Solids **35**, 501 (1974).
[17] O. V. Fat'yanov, R. L. Webb, and Y. M. Gupta, J. Appl. Phys. **97**, 123529 (2005).
[18] Y. M. Gupta, G. E. Duvall, and G. R. Fowles, J. Appl. Phys. **46**, 532 (1975).
[19] G. R. Fowles, J. Appl. Phys. **32**, 1475 (1961).
[20] I. J. Fritz, J. Appl. Phys. **45**, 60 (1974).
[21] V. A. Skudnov *et al.*, Metal Sci. Heat Treat. **11**, 981 (1969).
[22] J. O. Kane and R. F. Smith, AIP Conf. Proc. **845**, 244 (2006).
[23] A. K. Singh, High Press. Res. **4**, 336 (1990).